Cerebral Glucose Metabolism on Positron Emission Tomography of Children

Zuyao Y. Shan[1], Andrew J. Leiker[2], Arzu Onar[3], Yimei Li[3], Tianshu Feng[3], Wilburn E. Reddick[4], David C. Reutens[1], Barry L. Shulkin[5]

[1]Centre for Advanced Imaging, University of Queensland, Brisbane St Lucia, QLD 4072, Australia; [2]Physics and Mathematics, Fort Hays State University, Hays, Kansas 67601, USA; [3]Department of Biostatistics, St. Jude Children's Research Hospital, Memphis, TN 38105, USA; [4]Division of Translational Imaging Research, [5]Division of Nuclear Medicine, Department of Radiological Sciences, St. Jude Children's Research Hospital, Memphis, TN 38105, USA

Correspondence: Zuyao Shan, PhD
Centre for Advanced Imaging
University of Queensland
Brisbane St Lucia, QLD 4072, Australia
Telephone: +61-7-334-69026
E-mail: zuyao.shan@cai.uq.edu.au

Short Title: Brain Glucose Metabolism on Children PET

Key words: Child Development, Brain Imaging, Glucose Metabolism, FDG-PET, SUVs

Grant Support: This work is supported by the Cancer Center Support Grant (CA21765) from the National Cancer Institute and by the American Lebanese Syrian Associated Charities (ALSAC).

Addresses for reprint request: Zuyao Shan, PhD, Centre for Advanced Imaging, University of Queensland, Brisbane St Lucia, QLD 4072, Australia; e-mail: zuyao.shan@cai.uq.edu.au

Abstract

Establishing the normative range of age-dependent fluorodeoxyglucose (FDG) uptake in the developing brain is necessary for understanding regional quantitative analysis of positron emission tomography (PET) brain images in children and also to provide functional information on brain development. We analyzed head sections of FDG PET/CT images for 115 patients (5 months to 23 years old) without central nervous system disease before treatment, as PET studies are not performed on healthy children due to ethical considerations and the risk of radiation exposure. We investigated the changes in FDG uptake and established age-associated normative ranges of cerebral FDG. Head sections of FDG PET/CT images were registered to a population-based probabilistic atlas of human cortical structures. Gray matter of 56 brain structures were defined on normalized PET images according to the atlas. To avoid individual and experimental confounding factors, the relative standardized uptake value (SUV) over the cerebellum of each structure was calculated. Relative SUVs were analyzed by ANOVA and modeled using generalized estimating equalization (GEE) analysis with false discovery rate (FDR) control. Age and structure were significant factors affecting SUVs. Anatomic proximity had little effect on FDG uptake. Linear and quadratic developmental trajectories were observed on absolute and relative SUVs, respectively. An increase from posterior-to-anterior and superior to inferior pattern was observed in both absolute SUV increase rate and relative SUV peak age. The SUV of each structure was modeled with respect to age, and these models can serve as baselines for the quantitative analysis of cerebral FDG-PET images of children.

Introduction

In recent years, positron emission tomography (PET) with [^{18}F] fluoro-2-deoxy-D-glucose (FDG) has emerged as a useful imaging modality to study cellular metabolism in health and disease (Carson et al., 1998; Phelps, 2004) and acquire quantitative data on metabolism of the human brain (Phelps et al., 1979). Documentation of changes in cerebral metabolic activity during development is important not only to understand brain development and provide additional neuroscience-related information but also to increase the sensitivity and objectivity of the image-related diagnosis of diseases by enabling semi quantitative comparison to standard images.

However, the quantitative analysis of FDG-PET data from children remains challenging. It is difficult to establish a normal baseline of FDG uptake in children, as PET studies are not performed on healthy children because of ethical considerations and the risk of radiation exposure. Therefore, instead of using quantitative brain metabolism data from children, one often has to rely on data from normal adults for statistical mapping studies and to empirically discern disease.

The complex developmental changes in the anatomy of a child's brain have been well documented (Caviness et al., 1996; Lenroot and Giedd, 2006; Shaw et al., 2006; Shaw et al., 2008; Sowell et al., 2002; Sowell et al., 2004; Sowell and Jernigan, 1998; Thompson et al., 2005; Toga et al., 2006). Although the brain reaches 95% of its maximum size by 6 years, cortical and subcortical components of the brain change substantially during childhood and adolescence (Lenroot and Giedd, 2006). Complex cubic, quadratic, or linear developmental trajectories of cortical thickness have been observed in different

regions of the brain (Shaw et al., 2008), and changes in these trajectories have been correlated with changes in cognitive functions (Shaw et al., 2006). Generally, the maturation of regions of the brain responsible for higher cognitive functions such as attention, working memory, and executive functioning, continue into adolescence, whereas regions responsible for more primitive functions mature earlier (Benes et al., 1994; Toga et al., 2006). There is also a complex pattern of cortical maturation from the rostral-lateral-ventral pole to the dorsal-medial-caudal pole (Gogtay et al., 2004; Toga et al., 2006).

However, there are relatively few studies on changes in the metabolism of the developing brain(Chugani et al., 1987; Chugani, 1998; Gogtay et al., 2004; Kang et al., 2004; Kinnala et al., 1996; Muzik et al., 1999; Suhonenpolvi et al., 1995; Van Bogaert et al., 1998). Several studies (Chugani et al., 1987; Chugani, 1998; Kinnala et al., 1996; Muzik et al., 1999) found that the local cerebral metabolic rate of glucose (LCMRGlc) for various regions increases from birth (when the rate is lower than that of adults) until the child is 4 years old (when the rate is twice that of adults), and this high rate is maintained until 10 years of age. This is followed by a gradual decrease of LCMRGlc to reach the levels of adults by age 16–18 years. More recent studies (Kang et al., 2004; Van Bogaert et al., 1998) adjusted regional metabolism to global cerebral activities. Van Bogaert et al. used statistical parametric mapping method in SPM96 software (Wellcome Department of Cognitive Neurology, Institute of Neurology, London) and compared regional metabolism on 42 subjects with idiopathic epilepsy aged 6 to 38 years. They found a nonlinear increase of adjusted glucose metabolism mainly before the age of 25 years that remained relatively stable thereafter. Kang et al. used volume of interest and

SPM to compare regional metabolism in deaf children aged from 1 to 15 years old. They observed linear increases of FDG uptake in the right dorsomedial frontal gyrus and bilateral inferior prefrontal/orbitofrontal, and decreases in the inferior temporal gyrus. To summarize, previous studies (Chugani et al., 1987; Chugani, 1998; Gogtay et al., 2004; Kang et al., 2004; Kinnala et al., 1996; Muzik et al., 1999; Suhonenpolvi et al., 1995; Van Bogaert et al., 1998) reported regional differences in age-associated changes in metabolic activity. However, detailed regional FDG uptake in a relatively large cohort of subjects remains elusive.

In this retrospective study, we investigated age-related changes in FDG uptake in the cortical gray matter (GM) in order to establish a normative range of age-dependent regional FDG uptake and to explore the metabolic changes in developing brains. Head sections of whole-body PET scans from 115 pediatric cancer patients (5 months to 23 years old) with no evidence of CNS disease were the subjects of this study. The regional standardized uptake values (SUVs) of 56 brain structures were examined, normalized to a reference structure (cerebellum), and compared to determine developmental patterns.

Materials and methods

Data Source

This retrospective study was approved by the Institutional Review Board and waiver of consent was obtained. Records from patients who underwent whole-body FDG-PET/CT scans in last 5 years were reviewed. Patients with known central nervous system (CNS) impairment were not included in this analysis. All selected patients had normal CNS function (no known impaired intellectual function) and neurologic examinations at

the time of study. In order to avoid any potential effect of chemotherapy upon (CNS) function, whole-body FDG-PET/CT scans from 140 patients were selected on the basis of the criteria that the FDG-PET/CT scan was obtained prior to initiation of oncologic treatment. Data from 25 patients were excluded because of difficulties in image processing (e.g., failure of spatial normalization), regardless of age or disease type. The regional standardized uptake values (SUVs) of PET scans from 115 patients (5 months to 23 years, median age 11.7) were examined. Table I summarizes patient demographics and disease details. Figure 1 shows the age distribution of the115 patients.

Fig. 1; Table I

Image Acquisition

For FDG-PET/computed tomography (CT) examinations, 0.15mCi(55.5MBq/kg) [18] F-FDG [maximum 12mCi(444MBq)] was injected intravenously in patients after an overnight fast or after a minimum 4-h fast for studies done in the afternoon. Blood glucose was determined to be normal prior to injection. Patients younger than 7 years of age received sedation for examinations. However, sedation was not initiated until 60 minutes following injection of FDG, by which time the FDG signal within the brain was stable. Patients stayed in a quiet, dark room after the injection and were encouraged to remain recumbent and relaxed. Transmission CT images for attenuation correction and lesion localization as well as PET emission images were acquired approximately one hour later, using a GE Discovery LS PET/CT system (GE Medical Systems, Waukesha,

WI). CT acquisition parameters were as follows: slice thickness 0.5cm, tube rotation 0.8s, table speed 1.5cm/rotation, pitch 1.5:1, 120kV, 90mA, with dose modulation. PET images were obtained from the top of the skull through the feet for 5min per bed position in 2D mode with a spatial resolution of 3.9 × 3.9 × 4.25mm. Images were reconstructed by using standard vendor-supplied software.

Image processing

Head sections of whole-body PET scans were manually separated from those of the rest of the body. Head PET images were normalized to LPBA 40, a probabilistic population-based brain atlas of human cortical structures in an average space of 452 subjects and labeled with 56 structures (Shattuck et al., 2008) (See reference for the structural definition and function). Spatial normalization was performed by an automated image registration toolkit (Woods et al., 1992; Woods et al., 1993), which used the ratio of image uniformity as the objective function. A linear transformation model was used in this study. The spatial normalization procedure was evaluated in a previous study (Shan, at al., 2011). The agreement of spatial normalization was evaluated qualitatively by visual inspection of normalized PET images overlaid on the brain atlas. Data from 25 subjects were excluded due to registration failure. After the normalization, GM voxels on PET images were defined according to LPBA 40. The FDG SUV (Standardized Uptake Value) (Oldendor, 1974; Woodard et al., 1975) of each defined voxel was calculated as follows:

$$SUV = \frac{\text{Radioactive tissue concentration}}{\text{Injected dose} \,/\, \text{Patient weight}} \quad (1)$$

The voxels were further classified into 56 regions according to LPBA 40. The mean, median, minimum, maximum, and standard deviation values of SUVs for each structure were calculated. After two biostatisticians (AO and YL) reviewed the results, the SUV median for each structure was chosen as the summary statistic, since it captures the average intensity without being substantially affected by outliers.

Statistical analyses

Structural SUVs were analyzed as both absolute values and normalized to the reference region (cerebellum in this study) to determine the significant factors. The SUVs of different regions were normalized to the cerebellum because cerebellum usually exhibits a relatively consistent metabolic rate (Kushner et al, 1987; Heiss et al, 1991). The lesion-to-cerebellum uptake ratios (LCR) were used clinically to discern the benign and malignant abnormalities (Jabour et al, 1993; Obrzut et al, 2007; Lowe et al, 2009). The patients with Hodgkin's disease were selected as a subgroup. The age-related distribution patterns of absolute and normalized SUVs of left middle frontal gyrus in this subgroup were compared with the whole group.

Structural difference: ANOVA was used to test the difference in absolute SUVs among brain GM structures. In this test, the null hypothesis is that all structures have the same median. To determine where the differences occur, Turkey groupings were used to distinguish the structures that varied from one another.

Covariate analysis: The covariates of gender and age were examined. The interaction between age and gender was also analyzed. A t-test with a Satterthwaite correction was used to test gender groups within each structure. Since age is a continuous covariate, Pearson and Spearman correlations were used to determine the relationship between age

and absolute SUVs. The interaction of age and gender was tested by type 3 GEE analysis (Zeger et al., 1988) on both absolute and normalized SUVs.

Developmental changes analysis: Univariate analysis and multivariate analyses were performed to investigate the developmental changes of absolute and normalized SUVs. In the univariate analysis, a simple linear regression model with heterogeneous variance was fit for each individual structure. The variance was constructed to incorporate the heterogeneity of increase of variation with age. GEE (Zeger et al., 1988), a multivariate analysis method, was also used to simultaneously model median SUVs from all regions of the brain. Each of the 115 patients has 56 specific structures. Repeated measures were used to account for within-subject correlation of SUVs. Based on scatter plots of the absolute and normalized SUV (Fig. 3), linear and quadratic equations were used to fit the absolute SUVs and normalized SUVs, respectively:

$$SUV_{ij} = \alpha_j + \beta_j * Age + \varepsilon_{ij} \quad (2)$$

$$SUV_{N,\ ij} = \alpha_j + \beta_j * Age + \delta_j * (Age)^2 + \varepsilon_{ij} \quad (3),$$

in which i = 1, 2…115 represents the subject and j = 1, 2…56 represents the structure. For diagnosis of the regression, the Cook's D and leverage were calculated; and the residuals were plotted against fitted values. The false discovery rate (FDR) controlled p values were calculated for multiple comparisons.

Results

Absolute SUVs

The absolute SUVs of the structures were summarized in the Table II. For each of the 56 structures, there was no significant difference between median SUV values in the left

and right hemispheres. There were statistically significant differences among structures, which were summarized in Figure 2. There were no specific patterns of difference; that is, it was possible for SUVs of structures in the same lobe to be significantly different and those of structures in the different lobe to be not significantly different.

Table II, Fig. 2

Although the age–gender interaction of type 3 GEE analysis of SUVs from all patients was at the threshold (*Pr* > *Chi-Square,* 0.045), the SUVs of each structure did not differ significantly between females and males when age was not considered. However, SUVs for each structure were significantly different ($P<0.001$) between females and males in the age group of 16–17 years. The other age groups were not analyzed because of the low number of female or male patients.

There was a linear relationship between absolute SUVs and age for all structures. Figure 3(a) illustrates the median SUVs of the left middle frontal gyrus, showing that SUVs of the left middle frontal gyrus increase with age. Similar patterns were observed for the other 55 structures. Results of the univariate and multivariate analyses were similar for all structures. Therefore, we simplified the SUV norms for all structures to a linear expression:

$$SUV_{ij} = \alpha_j + \beta_j * Age + \varepsilon_{ij} \quad (3),$$

in which *j* represents different structures. The diagnosis of regression (Cook's D and leverage for the data) showed there were no significant outliers. The residual versus fitted values plot did not show any systematic trend. The Pearson and Spearman correlation

coefficients of absolute SUVs of all the structures with age and the change rate β_j were summarized in the Table III and figure 4. For cortical structures, structures in the frontal lobes had the higher rate of change (β_j) than structures in other lobes ($P < 0.05$). Those results are consistent with known developmental, brain maturation patterns (Benes et al., 1994; Gogtay et al., 2004; Toga et al., 2006).

Table III. Fig. 3, Fig. 4

Normalized SUVs

The normalized SUVs for individual structures were summarized in Table II. The GEE model considered interaction between subjects and structures. Age (*Pr > Chi-Square,* 0.006), Age square (*Pr > Chi-Square,* 0.002), and structure (*Pr > Chi-Square, < 0.001)* had a significant effect on normalized SUVs. Gender did not have a significant effect, but the interaction term of gender and structure has (*Pr > Chi-Square,* 0.04), which means gender had a significant effect in some structures.

There are quadratic relationships between the normative SUVs and age. Figure 3(b) showed the scatter plot of the normative SUVs of the left middle frontal gyrus as a function of age. The other structures showed similar patterns. Peak age and significance levels were summarized in the Table III. Among all the structures, postcentral gyrus, left superior occipital gyrus, parahippocampal gyrus, lingual gyrus, insular cortex, caudate, and putamen did not significantly correlate with age. The peak age of normative SUV of individual structures were colored encoded in the 3D surface rendering in figure 5.

Figure 5

Subgroup with Hodgkin's disease

The absolute and normalized age-related distributions of the subgroup with Hodgkin's disease of the left middle frontal gyrus were the same as the whole group (Fig. 3c and 3d). A linear relationship between the absolute SUVs and the age was observed ($P < 0.01$). A quadratic relationship between the normalized SUVs and the age was found ($P < 0.05$).

Discussion

This study was conducted to establish normal ranges of cerebral FDG uptake in PET scans of children and to determine age-related changes of FDG uptake in developing brains. Our major findings are as follows. First, there were significant differences in SUV values among different brain structures and anatomic proximity had little effect. Second, age had a significant effect on SUV uptakes. There was a linear increase of absolute SUVs with age for all structures but at different rates. For normalized regional SUVs with age, a quadratic relationship was observed for most structures. Third, normalized SUVs of regions associated with basic functions such as postcentral gyrus (primary somatosensory cortex), parahippocampal gyrus (scene recognition), lingual gyrus (dreaming and vision), and insular cortex (consciousness, emotion, and regulation of homeostasis) was not significantly correlated with age. Fourth, absolute and normalized SUV were modeled as linear and quadratic equations using GEE method.

Because of ethical considerations and the risk of radiation exposure, healthy children do not undergo PET scans. Therefore, we used images of head sections from whole-body PET scans for this study performed for non CNS malignancies. To avoid potential neurological toxicity from the treatment, we selected images that were acquired before start of therapy. We compared the subgroup with Hodgkin's disease with the whole group. The same age related distribution patterns were found in the subgroup as the whole group. The results suggested malignancies in the body do not significantly affect the brain FDG uptakes. AIR linear registration was used for normalization, because a previous registration evaluation study showed that AIR linear registration provides the highest tissue concordance among all methods evaluated (Shan et al., 2011). The averaged gray matter concordance measured as similarity index is 0.71, which suggested that the spatial normalization is acceptable for structures at the sub-lobular level. SUVs were calculated to exclude individual differences in weight and injected dose (Oldendor, 1974; Woodard et al., 1975). Because of the large data sample, the median SUV for each structure was used for analysis to avoid effects of possible outliers. To investigate the developmental changes and to avoid other confounding factors such as bloodstream, distribution of tracer in different body compartments, and potential impact of active tumor in body on the brain glucose uptakes, we normalized SUVs of brain structures to the cerebellum SUV in each subject.

We observed significant differences among different brain structures, which is consistent with results of previous studies (Chugani et al., 1987; Chugani, 1998; Gogtay et al., 2004; Kang et al., 2004; Kinnala et al., 1996; Muzik et al., 1999; Suhonenpolvi et al., 1995; Van Bogaert et al., 1998) and documented age-related structural changes in

developing brains (Caviness et al., 1996; Lenroot and Giedd, 2006; Shaw et al., 2006; Shaw et al., 2008; Sowell et al., 2002; Sowell et al., 2004; Sowell and Jernigan, 1998; Thompson et al., 2005; Toga et al., 2006). There were significant differences among structures in the same lobe, but not necessarily among structures in different lobes. These results suggest that anatomic proximity has little effect on SUVs of structures. Other factors such as biological function may determine SUVs of structures. The FDG SUV difference among structures may imply connectivity among maturing regions. However, this could be only explored by combination of structural MRI and fMRI data. There was no significant difference between structures of the left and right hemispheres, which further supports the validity of a traditional comparison of regional SUVs with matching contralateral regions.

SUVs did not significantly differ by gender without consideration of age. The age–gender interaction was at the threshold of statistical significance ($P = 0.04$) for both absolute and normalized SUVs. However, we did observe significantly different SUVs between females and males in a specific age group. We were able to study the age–gender interaction only for children aged 16 and 17 years since there was an insufficient number of subjects in other age groups. This result suggest that there may be difference in FDG uptake between females and males at the same age with females exhibiting a higher metabolic activity, which is consistent with findings from previous volumetric studies that females mature earlier than males.(Benes et al., 1994; Gogtay et al., 2004; Toga et al., 2006)

Age had a significant effect on SUV uptakes. Absolute SUVs of all structures increased with age until they reached the levels seen in normal adults. Univariate and

multivariate analyses showed similar age-related changes in absolute SUVs. For cortical structures, the frontal lobe showed the highest age-related absolute SUV change rate, followed by the parietal lobe, occipital lobe, and temporal lobe, although some structures (such as parahippocampal gyrus in the temporal lobe and gyrus rectus in the frontal lobe) stood out within the same lobe. The normalized SUVs showed a quadratic relationship with age. In other words, normalized SUVs increased with age to reach the peak and then decrease to a value slightly greater than the cerebellum SUVs. For cortical structures, structures in the frontal lobe (superior frontal gyrus) and temporal lobe (fusiform gyrus) had the greatest peak age among all structures. These findings were consistent with the well-known posterior-to-anterior and superior-to-inferior temporal brain developmental pattern. The frontal lobes do not fully mature until young adulthood. The regions associated with complex cognitive functions, such as the middle and inferior frontal gyrus, generally have a higher rate of change in SUVs and greater peak age than do other structures. Previous dynamic mapping studies of human cortical development have shown that parts of the brain associated with more basic functions mature early and those involved in executive function, attention, and motor coordination mature later (Gogtay et al., 2004; Lenroot and Giedd, 2006). Thus, the sequence of changes in SUVs agrees with the brain maturation pattern and regionally relevant milestones in cognitive and functional development.

We found that normalized regional SUVs demonstrated a quadratic relationship with age, which was consistent to results of some previous studies (Chugani et al., 1987; Chugani, 1998; Kinnala et al., 1996; Muzik et al., 1999). The finding of linear increases in absolute SUV changes with age is consistent with those of two recent studies (Kang et

al., 2004; Van Bogaert et al., 1998). Although previous studies (Chugani et al., 1987; Chugani, 1998; Kinnala et al., 1996; Muzik et al., 1999) measured LCMRGlc, there is a good correlation between SUV and LCMRGlc (r = 0.83, P< 0.001) (Suhonenpolvi et al., 1995). The previous studies (Chugani et al., 1987; Chugani, 1998) on LCMRGlc interpreted metabolic changes as the increase in LCMRGlc between birth and 4 years, which represents synaptic proliferation in the cerebral cortex. The high metabolic rate during age 4 to 10 years represents the period of synaptic excess and exuberant connectivity associated with a higher energy requirement by the cortex than in adults; LCMRGlc begins to decline with synaptic elimination after the age of 10 years. We observed a similar developmental pattern of normalized SUVs with an increase in young age (< 10 years old) and then decrease after 10-13 years old, but not so with the absolute SUVs. Therefore, Our findings suggested that normalized SUVs are more consistent with LCMRGlc than absolute SUVs.

We observed similar peak ages for structures associated with more basic functions, such as the superior parietal gyri. However, structures associated with more complex cognitive function had peak ages of 12 to 14 years old, such as superior parietal gyrus of about 10, middle frontal gyrus of about 13, and inferior temporal gyrus of 12 years. This finding aligned well with a recent longitudinal anatomic study of 145 children and adolescents, which showed a second wave of overproduction of the gray matter at approximately 11 years in girls and 12 years in boys (Giedd et al., 1999). Indeed, anatomic studies (Besl and Mckay, 1992; Caviness et al., 1996; Giedd et al., 1999; Lenroot and Giedd, 2006; Shaw et al., 2006; Shaw et al., 2008; Sowell et al., 2002; Sowell et al., 2004; Sowell and Jernigan, 1998; Thompson et al., 2005; Toga et al., 2006)

have suggested that the cortex area, which is associated with complex cognitive function, continues to mature until adolescence. The age-related SUV changes and rate of change found in our study agreed with these findings. Thus, our results suggested that the metabolic rate in the developing brain changes as the brain matures. If we assumed that the maturing areas need more energy than stable areas, the areas associated with complex functions mature later than those with basic functions, which are reflected by the higher SUV change rate in the former area. Although more energy is needed in maturing than matured areas during brain development, the overall SUV in the developing brain is still lower than that in the adult brain. This suggested that not only neurons and neural fibers but also support tissues (such as blood vessels or capillary vessels) are involved in development.

One of the main purposes of this study was to establish a norm for quantitative analysis of FDG-PET images of children. The diagnostic regression measurements suggest that the models of SUV for each structure fit the data well. To best of our knowledge, this is the first report of a model that describes age associated structural SUV uptakes. This model could be used as a reference for semi quantitative comparisons to discern abnormal regions in PET imaging.

This study is limited by its retrospective design and the fact that healthy children do not undergo PET scans. Images were acquired routinely as part of whole body imaging rather than dedicated cerebral imaging. Two assumptions have been made for this study: (1) SUVs calculated from head sections of “body” scans are the same as those from dedicated brain PET scans (a limited comparison of patients who underwent dedicated cerebral imaging followed by routine whole body imaging, including the head, showed

similar semi quantitative findings,) and (2) SUVs of the brain are normal in patients with tumors outside the CNS. As pertains to most retrospective studies, multi-institutional studies would be useful to confirm these results.

Conclusion

We investigated the SUVs of 56 brain structures based on whole-body PET images from 115 pediatric patients with tumors outside the CNS. SUVs differed by brain structure and age. Anatomic proximity had negligible effect on FDG uptakes. There were no significant differences between structures in the left and right hemispheres, suggesting that the traditional comparison of SUVs of any structure to its contralateral side is acceptable. We observed a linear increase of absolute SUV with age and quadratic relationship between normalized SUVs and age. The rate of regional absolute SUV increase and peak age of normalized SUVs was consistent with the maturation sequence observed in quantitative anatomic MR studies. The SUV of each structure was modeled with respect to age, and these models can be used as a baseline for quantitative analysis of FDG-PET images of children.

Acknowledgments

This work is supported by the Cancer Center Support Grant (CA21765) from the National Cancer Institute and by the American Lebanese Syrian Associated Charities (ALSAC).

Figure legends

Fig. 1. Age distribution of patients (N = 115) in the study. The female and male subjects were separated and shown on the left and right columns of the figure, respectively.

Fig. 2. Scatter plot of median absolute (a) and normalized (b) SUVs of the left middle frontal gyrus for patients (N = 115) and median absolute (c) and normalized (d) SUVs for the subgroup with Hodgkin's disease (N = 60). The scatter plot of median absolute SUV of the left middle frontal gyrus increases linearly with age (a and c). The scatter plot of normalized SUV of the left middle frontal gyrus with age shows a quadratic relationship (c and d). Similar patterns were observed for the other 55 structures. The same patterns were observed for the subgroup with Hodgkin's disease and the whole group.

Fig. 3. Differences of median SUVs between 2 structures across all ages and patients. There was no significant difference between 2 structures under any solid line, but there was a significant difference between 2 structures not under a solid line. For example, there was no significant difference between the L_middle frontal_G and R_middle frontal_G (L, left; G, gyrus; R, right), but there was a significant difference between L-middle frontal_G and L_middleorbitofrontal_G.

Fig. 4. Summary of the age-related change rate for different structures. The structures were clustered into different colors according to lobes. Structures in the frontal lobe showed the highest age-related absolute SUV change rate than structures in other lobes,

although some structures (such as parahippocampal gyrus in the temporal lobe and gyrus rectus in the frontal lobe) stood out within the same lobe.

Fig. 5. The surface rendering of normalized SUV peak ages overlaid on the atlas for individual structures. Peak ages were overlaid on a surface based representation of the MNI canonical brain using the SPM surfrend toolbox (written by I. Kahn; spmsurfrend.sourceforge.net) and NeuroLens (www.neurolens.org), separately for lateral (left column) and medial views (right column) in the left (upper row) and right hemispheres (lower row). The structures with no significant relationship with age were excluded. The peak ages were scaled into colors from green to yellow, and red (bottom color bar). The peak age is increased from posterior to anterior and from superior to inferior, which aligns well with brain maturation pattern found from brain anatomic studies.

Reference:

Benes FM, Turtle M, Khan Y, Farol P. (1994): Myelination of A Key Relay Zone in the Hippocampal-Formation Occurs in the Human Brain During Childhood, Adolescence, and Adulthood. Archives of General Psychiatry 51:477-484.

Besl PJ, Mckay ND. (1992): A Method for Registration of 3-D Shapes. IEEE Transactions on Pattern Analysis and Machine Intelligence 14:239-256.

Carson RE, Daube-Witherspoon ME, Herscovitch P. 1998. Quantitative Functional Brain Imaging with Postron Emission Tomography. San Diego:Academic Press.

Caviness VS, Kennedy DN, Richelme C, Rademacher J, Filipek PA. (1996): The human brain age 7-11 years: A volumetric analysis based on magnetic resonance images. Cerebral Cortex 6:726-736.

Chugani HT (1998): A critical period of brain development: Studies of cerebral glucose utilization with PET. Preventive Medicine 27:184-188.

Chugani HT, Phelps ME, Mazziotta JC. (1987): Positron Emission Tomography Study of Human-Brain Functional-Development. Annals of Neurology 22:487-497.

Giedd JN, Blumenthal J, Jeffries NO, Castellanos FX, Liu H, Zijdenbos A, Paus T, Evans AC, Rapoport JL. (1999): Brain development during childhood and adolescence: a longitudinal MRI study. Nature neurosicence 2:861-863.

Gogtay N, Giedd JN, Lusk L, Hayashi KM, Greenstein D, Vaituzis AC, Nugent TF, Herman DH, Clasen LS, Toga AW, Rapoport JL, Thompson PM. (2004): Dynamic mapping of human cortical development during childhood through early adulthood. Proceedings of the National Academy of Sciences of the United States of America 101:8174-8179.

Heiss WD, Szelies B, Kessler J, Herholz K. (1991): Abnormalities of energy metabolism in Alzheimer's disease studied with PET. Ann NY Acad Sci 640:65–71.

Jabour BA, Choi Y, Hoh CK, Rege SD, Soong JC, Lufkin RB, Hanafee WN, Maddahi J, Chaiken L, Bailet J, et al. (1993): Extracranial head and neck: PET imaging with 2-[F-18]fluoro-2-deoxy-D-glucose and MR imaging correlation. Radiology 186: 27-35.

Kang EJ, Lee DS, Kang HJ, Lee JS, Oh SH, Lee MC, Kim, CS. (2004): Age-associated changes of cerebral glucose metabolic activity in both male and female deaf children: parametric analysis using objective volume of interest and voxel-based mapping. NeuroImage 22: 1543-1553.

Kinnala A, Suhonenpolvi H, Aarimaa T, Kero P, Korvenranta H, Ruotsalainen U, Bergman J, Haaparanta M, Solin O, Nuutila P, Wegelius U. (1996): Cerebral metabolic rate for glucose during the first six months of life: An FDG positron emission tomography study. Archives of Disease in Childhood 74:F153-F157.

Kushner M, Tobin M, Alavi A, Chawluk J, Rosen M, Fazekas F, et al. (1987): Cerebellar glucose consumption in normal and pathologic states using fluorine-FDG and PET. J Nucl Med 28:1667–1670.

Lenroot RK, Giedd JN. (2006): Brain development in children and adolescents: Insights from anatomical magnetic resonance imaging. Neuroscience and Biobehavioral Reviews 30:718-729.

Lowe VJ, Kemp BJ, Jack CR Jr, Senjem M, Weigand S, Shiung M, Smith G, Knopman D, Boeve B, Mullan B, Petersen RC. (2009): Comparison of 18F-FDG and PiB PET in cognitive impairment. J Nucl Med 50:878-886.

Muzik O, Janisse J, Ager J, Shen CG, Chugani DC, Chugani HT. (1999): A mathematical model for the analysis of cross-sectional brain glucose metabolism data in children. Progress in Neuro-Psychopharmacology & Biological Psychiatry 23:589-600.

Obrzut S, Pham RH, Vera DR, Badran K, Hoha CK. (2007): Comparison of lesion-to-cerebellum uptake ratios and standardized uptake values in the evaluation of lung nodules with 18F-FDG PET. Nucl Med Commun 28:7-13.

Oldendor WH. (1974):Expression of Tissue Isotope Distribution. Journal of Nuclear Medicine 15:725-726.

Phelps ME, Huang SC, Hoffman EJ, Selin C, Sokoloff L, Kuhl DE. (1979): Tomographic Measurement of Local Cerebral Glucose Metabolic-Rate in Humans with (F-18)2-Fluoro-2-Deoxy-D-Glucose - Validation of Method. Annals of Neurology 6:371-388.

Phelps ME. 2004. PET: Molecular Imaging and Its Biological Applications. New York: Springer.

Shan ZY, Mateja S, Reddick WE, Glass JO, Shulkin BL. (2011): Retrospective Evaluation of PET-MRI Registration Algorithms. J of Digital Imaging, 24:485-493.

Shattuck DW, Mirza M, Adisetiyo V, Hojatkashani C, Salamon G, Narr KL, Poldrack RA, Bilder RM, Toga AW. (2008): Construction of a 3D probabilistic atlas of human cortical structures. NeuroImage 39:1064-1080.

Shaw P, Greenstein D, Lerch J, Clasen L, Lenroot R, Gogtay N, Evans A, Rapoport J, Giedd J, (2006): Intellectual ability and cortical development in children and adolescents. Nature 440:676-679.

Shaw P, Kabani NJ, Lerch JP, Eckstrand K, Lenroot R, Gogtay N, Greenstein D, Clasen L, Evans A, Rapoport JL, Giedd JN, Wise SP. (2008): Neurodevelopmental trajectories of the human cerebral cortex. Journal of Neuroscience 28:3586-3594.

Sowell ER, Jernigan TL. (1998): Further MRI evidence of late brain maturation: Limbic volume increases and changing asymmetries during childhood and adolescence. Developmental Neuropsychology 14:599-617.

Sowell ER, Thompson PM, Leonard CM, Welcome SE, Kan E, Toga AW. (2004): Longitudinal mapping of cortical thickness and brain growth in normal children. Journal of Neuroscience 24:8223-8231.

Sowell ER, Trauner DA, Gamst A, Jernigan TL. (2002): Development of cortical and subcortical brain structures in childhood and adolescence: a structural MRI study. Developmental Medicine and Child Neurology 44:4-16.

Suhonenpolvi H, Ruotsalainen U, Kinnala A, Bergman J, Haaparanta M, Teras M, Makela P, Solin O, Wegelius U. (1995): FDG-PET in Early Infancy - Simplified Quantification Methods to Measure Cerebral Glucose-Utilization. Journal of Nuclear Medicine 36:1249-1254.

Thompson PM, Sowell ER, Gogtay N, Giedd JN, Vidal CN, Hayashi KM, Leow A, Nicolson R, Rapoport JL, Toga AW. (2005): Structural MRI and brain development. International Review of Neurobiology 67:285-323.

Toga AW, Thompson PM, Sowell ER. (2006): Mapping brain maturation. Trends in Neurosciences 29:148-159.

Van Bogaert P, Wikler D, Damhaut P, Szliwowski HB, Goldman S. (1998): Regional changes in glucose metabolism during brain development from the age of 6 years. NeuroImage 8:62-68.

Woodard HQ, Bigler RE, Freed B, Russ G. (1975): Expression of Tissue Isotope Distribution - Comment. Journal of Nuclear Medicine 16:958-959.

Woods RP, Cherry SR, Mazziotta JC. (1992): Rapid Automated Algorithm for Aligning and Reslicing PET Images. Journal of Computer Assisted Tomography 16:620-633.

Woods RP, Mazziotta JC, Cherry SR. (1993): MRI-PET Registration with Automated Algorithm. Journal of Computer Assisted Tomography 17:536-546.

Zeger SL, Liang K, Albert PS. (1988): Models for Longitudinal Data: A Generalized Estimating Equation Approach. Biometrics 44:1049-1060.

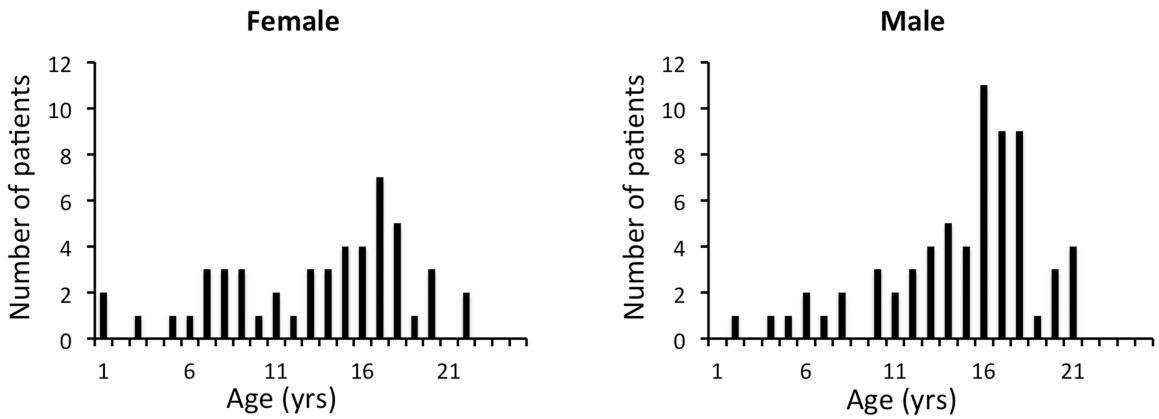

Fig. 1. Age distribution of patients (N = 115) in the study. The female and male subjects were separated and shown on the left and right columns of the figure, respectively.

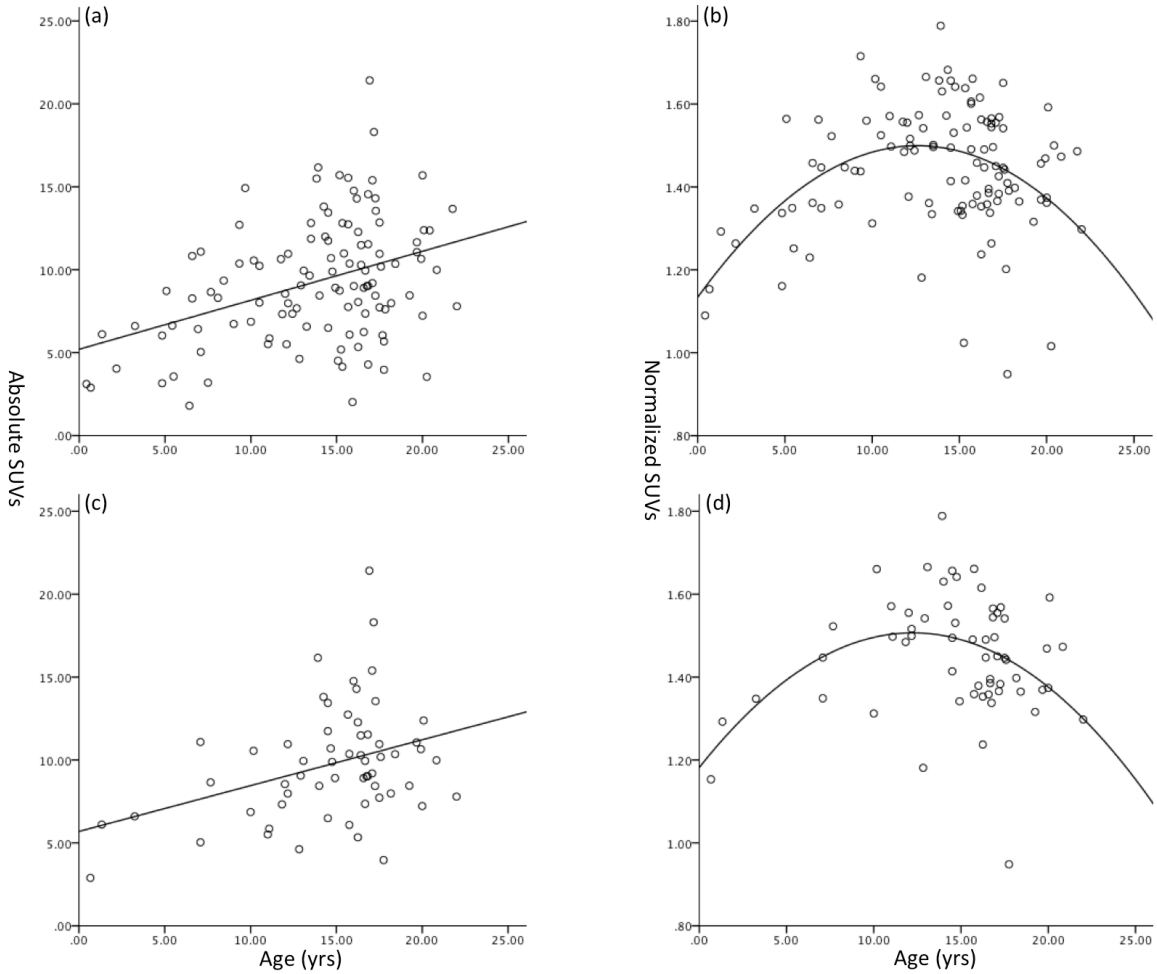

Fig. 2. Scatter plot of median absolute (a) and normalized (b) SUVs of the left middle frontal gyrus for patients (N = 115) and median absolute (c) and normalized (d) SUVs for the subgroup with Hodgkin's disease (N = 60). The scatter plot of median absolute SUV of the left middle frontal gyrus increases linearly with age (a and c). The scatter plot of normalized SUV of the left middle frontal gyrus with age shows a quadratic relationship (c and d). Similar patterns were observed for the other 55 structures. The same patterns were observed for the subgroup with Hodgkin's disease and the whole group.

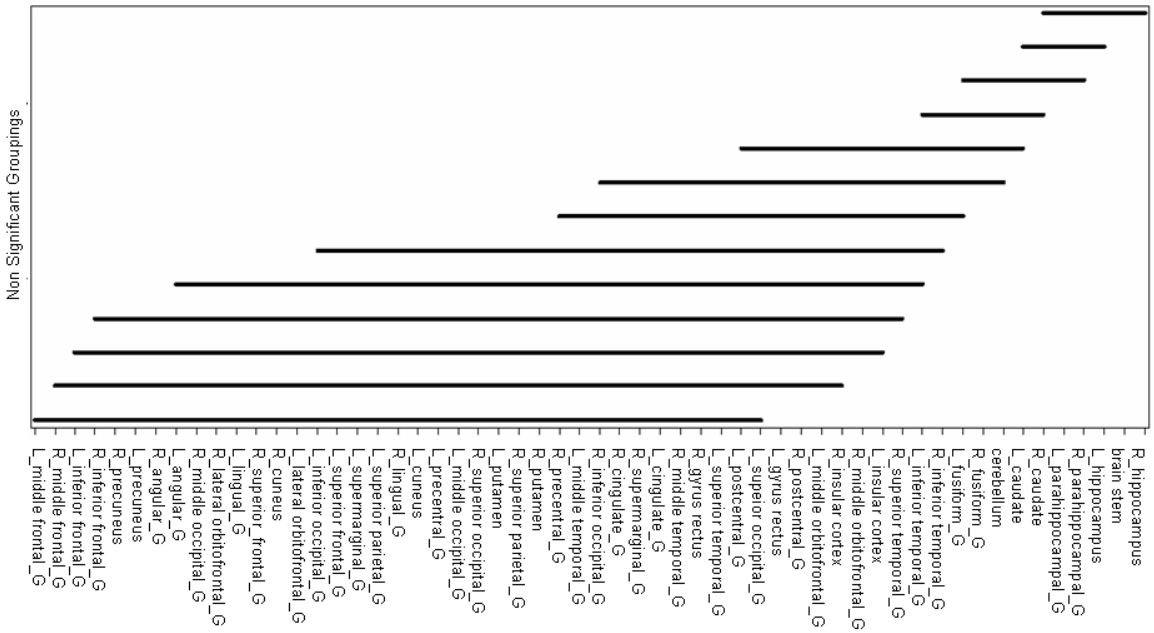

Fig. 3. Differences of median SUVs between 2 structures across all ages and patients. There was no significant difference between 2 structures under any solid line, but there was a significant difference between 2 structures not under a solid line. For example, there was no significant difference between the L_middle frontal_G and R_middle frontal_G (L, left; G, gyrus; R, right), but there was a significant difference between L-middle frontal_G and L_middleorbitofrontal_G.

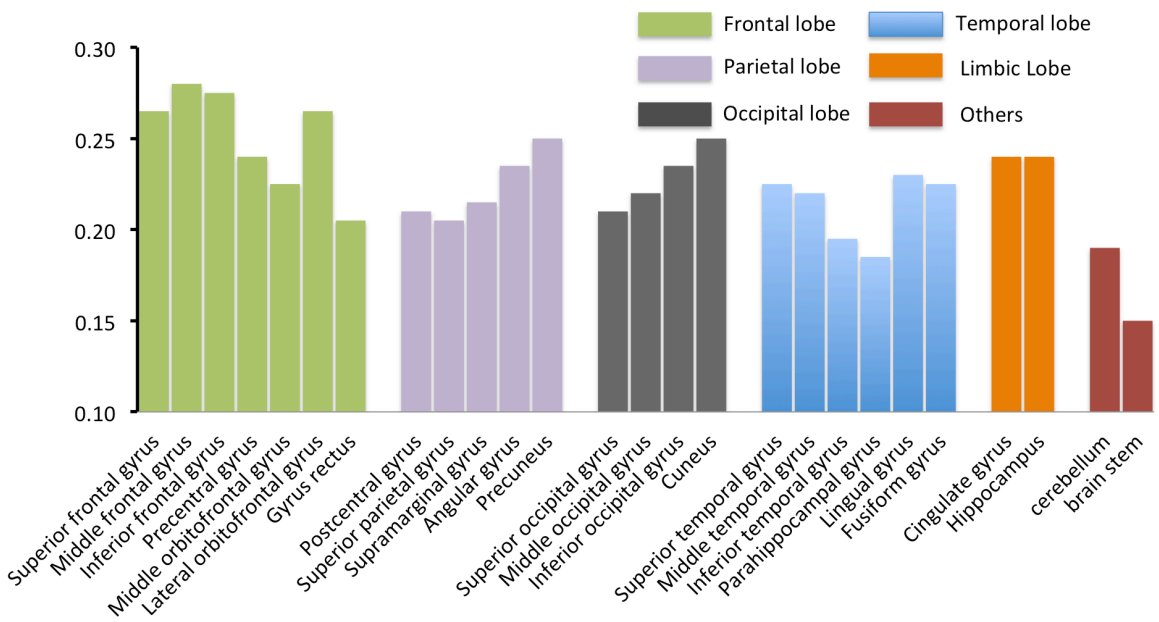

Fig. 4. Summary of the age-related change rate for different structures. The structures were clustered into different colors according to lobes. Structures in the frontal lobe showed the highest age-related absolute SUV change rate than structures in other lobes, although some structures (such as parahippocampal gyrus in the temporal lobe and gyrus rectus in the frontal lobe) stood out within the same lobe.

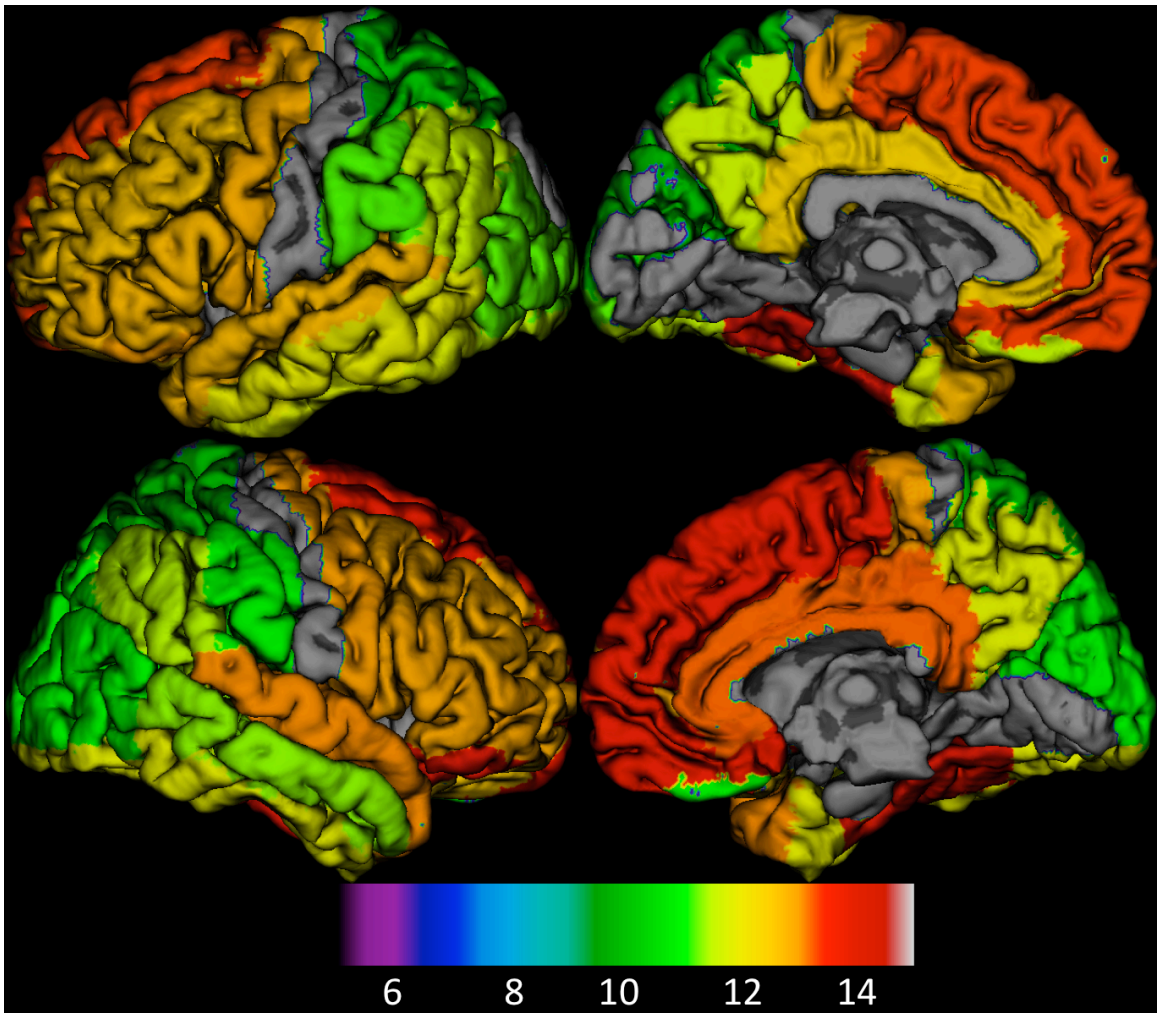

Fig. 5. The surface rendering of normalized SUV peak ages overlaid on the atlas for individual structures. Peak ages were overlaid on a surface based representation of the MNI canonical brain using the SPM surfrend toolbox (written by I. Kahn; spmsurfrend.sourceforge.net) and NeuroLens (www.neurolens.org), separately for lateral (left column) and medial views (right column) in the left (upper row) and right hemispheres (lower row). The structures with no significant relationship with age were excluded. The peak ages were scaled into colors from green to yellow, and red (bottom color bar). The peak age is increased from posterior to anterior and from superior to inferior, which aligns well with brain maturation pattern found from brain anatomic studies.

Table I Summary of the patient information

Gender	Etiology
Female (N= 52), mean age 12.77 yrs old	Peripheral neuroepithelioma, N = 6 Hodgkin's disease, N = 60 Malignant lymphoma, N = 17 Desmoid tumor, N = 18
Male (N = 63), mean age 13.85 yrs old	Rhabdomyosarcoma, N = 5 Others, N = 9

Table II Regional FDG uptakes in developing brain

Structures	L/R	Absolute SUVs (95% CIs)					Normalized SUVs (95% CIs)				
		0-5 (yrs)	5-10 (yrs)	10-15 (yrs)	15-20 (yrs)	20-25 (yrs)	0-5 (yrs)	5-10 (yrs)	10-15 (yrs)	15-20 (yrs)	20-25 (yrs)
Superior frontal gyrus	L	4.06 (2.63, 5.48)	7.10 (5.50, 8.70)	8.52 (7.61, 9.43)	8.97 (8.00, 9.94)	9.03 (5.66, 12.39)	1.09 (0.97, 1.21)	1.28 (1.23, 1.33)	1.36 (1.32, 1.40)	1.29 (1.26, 1.32)	1.27 (1.12, 1.43)
	R	4.12 (2.65, 5.60)	7.15 (5.53, 8.77)	8.59 (7.66, 9.51)	9.08 (8.09, 10.06)	9.29 (5.84, 12.74)	1.11 (0.98, 1.23)	1.29 (1.23, 1.35)	1.37 (1.33, 1.41)	1.31 (1.28, 1.34)	1.31 (1.16, 1.47)
Middle frontal gyrus	L	4.56 (3.06, 6.06)	8.03 (6.25, 9.81)	9.60 (8.53, 10.67)	9.97 (8.87, 11.08)	9.96 (5.99, 13.92)	1.23 (1.14, 1.33)	1.44 (1.37, 1.51)	1.53 (1.48, 1.58)	1.43 (1.39, 1.47)	1.39 (1.18, 1.61)
	R	4.46 (2.98, 5.95)	7.95 (6.06, 9.84)	9.44 (8.42, 10.47)	9.78 (8.70, 10.86)	9.67 (6.02, 13.32)	1.21 (1.11, 1.31)	1.42 (1.33, 1.50)	1.51 (1.46, 1.55)	1.40 (1.37, 1.44)	1.36 (1.18, 1.54)
Inferior frontal gyrus	L	4.44 (2.96, 5.91)	7.88 (6.11, 9.65)	9.26 (8.21, 10.31)	9.77 (8.68, 10.86)	9.66 (5.88, 13.44)	1.20 (1.10, 1.30)	1.42 (1.34, 1.50)	1.47 (1.43, 1.52)	1.40 (1.36, 1.44)	1.35 (1.15, 1.56)
	R	4.50 (3.02, 5.99)	7.91 (5.94, 9.88)	9.19 (8.19, 10.18)	9.65 (8.58, 10.73)	9.56 (6.12, 13.00)	1.22 (1.12, 1.32)	1.41 (1.32, 1.50)	1.47 (1.42, 1.51)	1.38 (1.35, 1.42)	1.35 (1.21, 1.50)
Precentral gyrus	L	4.28 (2.90, 5.66)	7.10 (5.55, 8.64)	8.27 (7.40, 9.13)	8.84 (7.91, 9.77)	8.83 (5.67, 12.00)	1.21 (1.11, 1.31)	1.42 (1.33, 1.50)	1.51 (1.46, 1.55)	1.40 (1.37, 1.44)	1.36 (1.18, 1.54)
	R	4.24 (2.86, 5.63)	6.97 (5.30, 8.65)	8.13 (7.30, 8.95)	8.64 (7.72, 9.57)	8.67 (5.76, 11.59)	1.15 (1.05, 1.25)	1.25 (1.18, 1.31)	1.31 (1.27, 1.34)	1.25 (1.22, 1.27)	1.24 (1.13, 1.35)
Middle orbitofrontal gyrus	L	3.95 (2.76, 5.15)	6.52 (5.09, 7.95)	7.62 (6.80, 8.44)	8.15 (7.25, 9.06)	8.28 (5.07, 11.48)	1.08 (1.02, 1.14)	1.19 (1.14, 1.23)	1.22 (1.19, 1.25)	1.17 (1.14, 1.20)	1.16 (1.00, 1.33)
	R	3.85 (2.67, 5.04)	6.46 (4.96, 7.96)	7.56 (6.77, 8.36)	8.07 (7.17, 8.97)	8.02 (4.94, 11.10)	1.05 (0.98, 1.12)	1.17 (1.11, 1.23)	1.21 (1.18, 1.24)	1.16 (1.13, 1.19)	1.13 (0.97, 1.28)
Lateral orbitofrontal gyrus	L	4.20 (2.85, 5.56)	7.27 (5.58, 8.95)	8.49 (7.52, 9.45)	9.07 (8.04, 10.09)	9.16 (5.52, 12.81)	1.14 (1.07, 1.21)	1.32 (1.24, 1.39)	1.35 (1.30, 1.40)	1.30 (1.27, 1.34)	1.29 (1.09, 1.48)
	R	4.35 (2.79, 5.90)	7.29 (5.51, 9.06)	8.60 (7.67, 9.52)	9.21 (8.15, 10.27)	9.29 (6.04, 12.54)	1.17 (1.04, 1.30)	1.31 (1.23, 1.39)	1.37 (1.34, 1.41)	1.32 (1.28, 1.36)	1.32 (1.20, 1.44)
Gyrus rectus	L	3.95 (2.65, 5.26)	6.73 (5.20, 8.25)	7.70 (6.88, 8.53)	8.14 (7.22, 9.07)	7.47 (4.71, 10.23)	1.07 (0.97, 1.17)	1.23 (1.18, 1.28)	1.23 (1.19, 1.28)	1.17 (1.13, 1.21)	1.06 (0.94, 1.18)
	R	4.19 (2.70, 5.67)	7.06 (5.45, 8.68)	8.03 (7.12, 8.94)	8.35 (7.38, 9.31)	7.50 (4.57, 10.43)	1.13 (1.00, 1.25)	1.29 (1.22, 1.35)	1.28 (1.23, 1.33)	1.20 (1.15, 1.24)	1.06 (0.90, 1.23)
Postcentral gyrus	L	4.29 (2.92, 5.67)	6.83 (5.31, 8.34)	7.72 (6.93, 8.51)	8.25 (7.38, 9.13)	8.30 (5.58, 11.03)	1.17 (1.07, 1.26)	1.24 (1.19, 1.29)	1.24 (1.21, 1.27)	1.19 (1.17, 1.22)	1.19 (1.11, 1.28)
	R	4.21 (2.90, 5.53)	6.66 (5.09, 8.23)	7.59 (6.85, 8.34)	8.10 (7.24, 8.95)	8.13 (5.53, 10.72)	1.15 (1.04, 1.26)	1.20 (1.14, 1.26)	1.22 (1.19, 1.26)	1.17 (1.15, 1.19)	1.17 (1.09, 1.25)
Superior parietal gyrus	L	4.52 (3.08, 5.97)	7.52 (5.79, 9.25)	8.42 (7.54, 9.30)	8.78 (7.81, 9.75)	8.66 (5.65, 11.66)	1.23 (1.12, 1.34)	1.35 (1.29, 1.42)	1.35 (1.30, 1.39)	1.26 (1.23, 1.30)	1.23 (1.13, 1.34)
	R	4.42 (3.07, 5.76)	7.41 (5.65, 9.17)	8.20 (7.39, 9.02)	8.53 (7.59, 9.46)	8.30 (5.60, 11.01)	1.20 (1.12, 1.28)	1.33 (1.25, 1.40)	1.32 (1.28, 1.36)	1.23 (1.20, 1.26)	1.19 (1.10, 1.28)
Supramarginal gyrus	L	4.39 (2.97, 5.80)	7.39 (5.73, 9.05)	8.40 (7.52, 9.29)	8.88 (7.92, 9.85)	8.74 (5.49, 11.98)	1.19 (1.09, 1.29)	1.34 (1.28, 1.40)	1.34 (1.30, 1.39)	1.28 (1.25, 1.31)	1.24 (1.09, 1.39)
	R	4.34 (2.93, 5.76)	7.12 (5.36, 8.88)	8.09 (7.29, 8.88)	8.40 (7.51, 9.30)	8.24 (5.52, 10.96)	1.18 (1.08, 1.28)	1.27 (1.19, 1.35)	1.30 (1.26, 1.34)	1.21 (1.18, 1.24)	1.18 (1.09, 1.27)
Angular gyrus	L	4.46 (3.00, 5.91)	7.69 (5.91, 9.47)	8.74 (7.81, 9.68)	9.17 (8.15, 10.19)	9.21 (5.82, 12.59)	1.21 (1.10, 1.32)	1.38 (1.30, 1.46)	1.40 (1.35, 1.44)	1.32 (1.28, 1.35)	1.30 (1.17, 1.44)
	R	4.47 (3.01, 5.94)	7.78 (5.91, 9.64)	8.87 (7.97, 9.77)	9.16 (8.16, 10.16)	8.98 (5.75, 12.21)	1.21 (1.11, 1.32)	1.39 (1.30, 1.47)	1.42 (1.38, 1.46)	1.32 (1.28, 1.35)	1.27 (1.12, 1.42)
Precuneus	L	4.67 (3.13, 6.21)	7.91 (6.08, 9.74)	9.14 (8.17, 10.12)	9.52 (8.49, 10.56)	9.61 (6.18, 13.04)	1.26 (1.17, 1.36)	1.43 (1.35, 1.50)	1.46 (1.42, 1.50)	1.37 (1.34, 1.41)	1.36 (1.21, 1.52)
	R	4.66 (3.12, 6.19)	7.93 (6.11, 9.76)	9.16 (8.19, 10.13)	9.54 (8.48, 10.60)	9.68 (6.25, 13.11)	1.26 (1.17, 1.35)	1.43 (1.36, 1.50)	1.46 (1.42, 1.51)	1.37 (1.34, 1.41)	1.37 (1.22, 1.53)
Superior occipital gyrus	L	4.27 (3.01, 5.53)	7.08 (5.39, 8.76)	7.63 (6.79, 8.46)	8.24 (7.31, 9.18)	7.95 (5.51, 10.39)	1.17 (1.08, 1.25)	1.27 (1.20, 1.35)	1.22 (1.17, 1.26)	1.18 (1.15, 1.21)	1.15 (1.08, 1.22)
	R	4.39 (2.95, 5.82)	7.36 (5.66, 9.07)	8.16 (7.31, 9.00)	8.67 (7.72, 9.62)	8.47 (5.54, 11.40)	1.19 (1.08, 1.30)	1.33 (1.25, 1.40)	1.31 (1.27, 1.35)	1.24 (1.21, 1.28)	1.21 (1.09, 1.33)
Middle occipital gyrus	L	4.38 (2.95, 5.80)	7.34 (5.64, 9.04)	8.19 (7.30, 9.07)	8.75 (7.79, 9.71)	8.64 (5.54, 11.75)	1.19 (1.08, 1.30)	1.31 (1.24, 1.39)	1.31 (1.26, 1.35)	1.26 (1.21, 1.30)	1.23 (1.10, 1.35)
	R	4.56 (3.00, 6.12)	7.74 (5.93, 9.55)	8.67 (7.76, 9.59)	9.06 (8.04, 10.08)	8.69 (5.58, 11.80)	1.23 (1.10, 1.37)	1.38 (1.29, 1.46)	1.39 (1.35, 1.43)	1.30 (1.26, 1.34)	1.23 (1.08, 1.39)
Inferior occipital gyrus	L	4.36 (3.03, 5.69)	7.45 (5.81, 9.10)	8.33 (7.44, 9.23)	8.94 (7.89, 9.98)	8.97 (5.51, 12.44)	1.19 (1.07, 1.31)	1.34 (1.25, 1.44)	1.33 (1.28, 1.38)	1.28 (1.23, 1.32)	1.27 (1.04, 1.50)
	R	3.97 (2.95, 5.00)	7.19 (5.52, 8.86)	7.97 (7.13, 8.80)	8.63 (7.65, 9.60)	7.90 (5.09, 10.70)	1.10 (1.00, 1.20)	1.29 (1.19, 1.39)	1.28 (1.23, 1.33)	1.24 (1.19, 1.28)	1.13 (0.90, 1.36)
Cuneus	L	4.21 (2.82, 5.60)	7.19 (5.44, 8.94)	8.22 (7.30, 9.15)	8.89 (7.87, 9.90)	8.76 (6.04, 11.49)	1.14 (1.00, 1.28)	1.29 (1.19, 1.39)	1.31 (1.26, 1.36)	1.27 (1.23, 1.31)	1.26 (1.15, 1.37)
	R	4.31 (2.83, 5.79)	7.52 (5.70, 9.35)	8.36 (7.45, 9.26)	9.04 (8.06, 10.02)	9.21 (6.01, 12.42)	1.16 (1.03, 1.29)	1.35 (1.24, 1.45)	1.34 (1.28, 1.39)	1.30 (1.26, 1.34)	1.31 (1.16, 1.46)
Superior temporal gyrus	L	4.03 (2.65, 5.41)	6.82 (5.30, 8.33)	7.78 (6.97, 8.60)	8.29 (7.41, 9.17)	8.55 (5.43, 11.66)	1.09 (0.98, 1.19)	1.24 (1.17, 1.31)	1.24 (1.21, 1.27)	1.20 (1.17, 1.23)	1.21 (1.06, 1.36)
	R	3.89 (2.57, 5.20)	6.52 (4.92, 8.12)	7.40 (6.66, 8.15)	7.91 (7.07, 8.75)	7.73 (5.32, 10.14)	1.05 (0.94, 1.16)	1.18 (1.10, 1.26)	1.19 (1.16, 1.22)	1.15 (1.12, 1.17)	1.11 (1.03, 1.20)
Middle temporal gyrus	L	4.15 (2.80, 5.51)	7.12 (5.55, 8.69)	8.08 (7.20, 8.96)	8.60 (7.64, 9.55)	8.71 (5.54, 11.88)	1.13 (1.04, 1.21)	1.29 (1.22, 1.36)	1.29 (1.25, 1.33)	1.24 (1.20, 1.27)	1.23 (1.07, 1.40)
	R	4.15 (2.76, 5.53)	7.11 (5.42, 8.79)	8.02 (7.19, 8.84)	8.34 (7.41, 9.28)	8.27 (5.47, 11.08)	1.12 (1.02, 1.22)	1.28 (1.20, 1.35)	1.28 (1.25, 1.32)	1.20 (1.17, 1.23)	1.18 (1.06, 1.29)
Inferior temporal gyrus	L	3.69 (2.58, 4.81)	6.07 (4.76, 7.37)	7.04 (6.31, 7.77)	7.51 (6.66, 8.36)	7.61 (4.99, 10.24)	1.01 (0.95, 1.07)	1.11 (1.06, 1.16)	1.13 (1.10, 1.16)	1.08 (1.05, 1.11)	1.09 (0.97, 1.20)
	R	3.58 (2.55, 4.62)	5.87 (4.45, 7.28)	6.79 (6.11, 7.47)	7.18 (6.38, 7.97)	7.03 (4.55, 9.52)	0.98 (0.93, 1.03)	1.06 (0.99, 1.13)	1.09 (1.06, 1.12)	1.03 (1.00, 1.07)	1.00 (0.89, 1.12)
Parahippocampal gyrus	L	2.58 (2.03, 3.14)	4.06 (3.21, 4.92)	4.82 (4.38, 5.26)	5.66 (5.09, 6.23)	5.78 (4.04, 7.52)	0.72 (0.66, 0.79)	0.76 (0.72, 0.80)	0.78 (0.76, 0.80)	0.83 (0.81, 0.85)	0.84 (0.76, 0.92)
	R	2.53 (1.91, 3.16)	3.99 (3.13, 4.85)	4.70 (4.29, 5.12)	5.48 (4.91, 6.05)	5.49 (3.93, 7.04)	0.70 (0.67, 0.74)	0.75 (0.70, 0.80)	0.76 (0.74, 0.78)	0.80 (0.78, 0.82)	0.80 (0.73, 0.87)
Lingual gyrus	L	4.75 (3.16, 6.35)	7.48 (5.71, 9.24)	8.45 (7.50, 9.39)	8.98 (7.94, 10.03)	9.03 (5.91, 12.15)	1.29 (1.13, 1.45)	1.35 (1.26, 1.44)	1.34 (1.29, 1.40)	1.28 (1.24, 1.32)	1.29 (1.15, 1.43)
	R	4.64 (3.16, 6.12)	7.39 (5.57, 9.21)	8.29 (7.33, 9.24)	8.83 (7.83, 9.83)	8.99 (5.97, 12.01)	1.26 (1.12, 1.40)	1.33 (1.23, 1.43)	1.32 (1.27, 1.37)	1.27 (1.23, 1.30)	1.28 (1.11, 1.46)
Fusiform gyrus	L	3.07 (2.27, 3.88)	5.31 (4.16, 6.46)	6.31 (5.68, 6.94)	7.07 (6.34, 7.81)	7.05 (4.62, 9.48)	0.85 (0.76, 0.95)	0.98 (0.92, 1.04)	1.02 (0.98, 1.05)	1.03 (0.99, 1.06)	1.01 (0.86, 1.17)
	R	3.01 (2.28, 3.73)	5.28 (4.07, 6.48)	6.31 (5.70, 6.92)	6.96 (6.23, 7.69)	6.94 (4.58, 9.30)	0.84 (0.75, 0.93)	0.97 (0.90, 1.04)	1.02 (0.98, 1.05)	1.01 (0.98, 1.05)	1.00 (0.84, 1.15)
Cingulate gyrus	L	4.02 (2.81, 5.22)	6.24 (4.86, 7.61)	7.42 (6.65, 8.19)	8.13 (7.27, 8.99)	8.15 (5.33, 10.97)	1.10 (1.03, 1.17)	1.15 (1.11, 1.19)	1.19 (1.15, 1.22)	1.18 (1.15, 1.20)	1.16 (1.06, 1.26)
	R	4.01 (2.81, 5.21)	6.33 (4.85, 7.80)	7.58 (6.82, 8.34)	8.16 (7.28, 9.03)	8.05 (5.50, 10.61)	1.10 (1.03, 1.16)	1.16 (1.11, 1.21)	1.22 (1.18, 1.25)	1.18 (1.16, 1.21)	1.16 (1.12, 1.20)
Hippocampus	L	4.21 (2.80, 5.62)	6.78 (5.21, 8.36)	7.94 (7.09, 8.80)	8.50 (7.57, 9.42)	8.47 (5.54, 11.40)	1.14 (1.03, 1.24)	1.24 (1.19, 1.28)	1.27 (1.23, 1.31)	1.23 (1.20, 1.26)	1.21 (1.08, 1.34)
	R	4.21 (2.77, 5.65)	6.78 (5.23, 8.33)	8.01 (7.13, 8.88)	8.58 (7.65, 9.51)	8.82 (5.65, 11.98)	1.14 (1.02, 1.25)	1.24 (1.19, 1.29)	1.28 (1.24, 1.32)	1.24 (1.21, 1.27)	1.25 (1.10, 1.41)
Insular cortex	L	3.06 (2.14, 3.98)	5.22 (4.09, 6.36)	5.93 (5.32, 6.53)	6.68 (6.01, 7.35)	7.01 (4.64, 9.37)	0.84 (0.77, 0.90)	0.97 (0.92, 1.03)	0.96 (0.91, 1.00)	0.98 (0.95, 1.01)	1.01 (0.89, 1.12)
	R	2.76 (1.94, 3.57)	4.80 (3.64, 5.95)	5.41 (4.82, 6.00)	6.07 (5.47, 6.66)	6.47 (4.38, 8.56)	0.75 (0.68, 0.82)	0.88 (0.81, 0.95)	0.87 (0.82, 0.92)	0.89 (0.86, 0.92)	0.94 (0.79, 1.09)
Caudate	L	4.31 (3.30, 5.32)	6.61 (5.17, 8.05)	7.91 (7.15, 8.68)	8.93 (7.96, 9.89)	9.00 (6.05, 11.94)	1.20 (1.14, 1.26)	1.24 (1.17, 1.30)	1.28 (1.23, 1.33)	1.30 (1.27, 1.34)	1.29 (1.23, 1.35)
	R	4.27 (3.21, 5.32)	6.49 (5.02, 7.95)	7.87 (7.11, 8.63)	8.91 (7.96, 9.86)	8.84 (6.25, 11.43)	1.18 (1.09, 1.28)	1.21 (1.14, 1.28)	1.27 (1.23, 1.32)	1.30 (1.27, 1.34)	1.28 (1.23, 1.34)
Putamen	L	2.49 (1.94, 3.04)	3.58 (2.84, 4.32)	4.28 (3.88, 4.69)	5.01 (4.45, 5.56)	5.12 (3.53, 6.72)	0.70 (0.63, 0.77)	0.68 (0.64, 0.71)	0.69 (0.67, 0.71)	0.73 (0.71, 0.75)	0.74 (0.69, 0.79)
	R	2.53 (1.94, 3.11)	3.56 (2.79, 4.32)	4.26 (3.88, 4.64)	4.89 (4.37, 5.42)	4.96 (3.52, 6.40)	0.70 (0.65, 0.76)	0.67 (0.63, 0.71)	0.69 (0.67, 0.71)	0.71 (0.70, 0.73)	0.72 (0.67, 0.77)
Cerebellum	NA	3.63 (2.67, 4.59)	5.45 (4.27, 6.62)	6.22 (5.62, 6.83)	6.90 (6.18, 7.62)	6.91 (4.80, 9.03)	1.00 (1.00, 1.00)	1.00 (1.00, 1.00)	1.00 (1.00, 1.00)	1.00 (1.00, 1.00)	1.00 (1.00, 1.00)
Brain stem	NA	2.48 (1.96, 3.00)	3.53 (2.78, 4.28)	4.24 (3.88, 4.60)	4.96 (4.47, 5.45)	4.82 (3.50, 6.14)	0.70 (0.60, 0.79)	0.67 (0.62, 0.71)	0.69 (0.66, 0.71)	0.73 (0.71, 0.74)	0.71 (0.66, 0.75)

Table III Age related FDG uptake changes in developing brain[†]

Lobes	Structures	L/R	Absolute SUVs			Normalized SUVs	
			r	ρ	β_j	Peak Age	FDR-q
Frontal Lobe	Superior frontal gyrus	L	0.36	0.31	0.26	13.32	<0.001
		R	0.36	0.31	0.27	13.75	<0.001
	Middle frontal gyrus	L	0.34	0.28	0.28	12.59	<0.001
		R	0.34	0.30	0.28	12.83	<0.001
	Inferior frontal gyrus	L	0.34	0.29	0.28	12.73	<0.001
		R	0.34	0.30	0.27	12.9	<0.001
	Precentral gyrus	L	0.35	0.31	0.24	12.83	<0.001
		R	0.35	0.31	0.24	12.99	0.002
	Middle orbitofrontal gyrus	L	0.34	0.30	0.23	12.44	<0.001
		R	0.34	0.30	0.22	12.51	<0.001
	Lateral orbitofrontal gyrus	L	0.34	0.30	0.26	12.98	<0.001
		R	0.35	0.32	0.27	14.13	<0.001
	Gyrus rectus	L	0.31	0.26	0.21	11.56	<0.001
		R	0.28	0.22	0.20	10.95	<0.001
Parietal Lobe	Postcentral gyrus	L	0.32	0.29	0.21	NA	0.06
		R	0.33	0.30	0.21	NA	0.3
	Superior parietal gyrus	L	0.29	0.24	0.21	10.11	<0.001
		R	0.28	0.24	0.20	9.9	<0.001
	Supramarginal gyrus	L	0.31	0.26	0.22	11.18	<0.001
		R	0.31	0.26	0.21	10.86	<0.001
	Angular gyrus	L	0.31	0.26	0.24	11.62	<0.001
		R	0.31	0.26	0.23	11.48	<0.001
	Precuneus	L	0.32	0.26	0.25	11.67	<0.001
		R	0.32	0.27	0.25	11.88	<0.001
Occipital lobe	Superior occipital gyrus	L	0.30	0.27	0.20	NA	0.1
		R	0.31	0.27	0.22	10.9	0.005
	Middle occipital gyrus	L	0.31	0.27	0.22	11.21	0.008
		R	0.29	0.25	0.22	10.91	0.001
	Inferior occipital gyrus	L	0.31	0.27	0.24	11.59	0.07
		R	0.32	0.28	0.23	11.93	0.005
	Cuneus	L	0.33	0.31	0.25	10.11	0.01
		R	0.34	0.30	0.25	10.8	0.02
Temporal lobe	Superior temporal gyrus	L	0.34	0.30	0.23	12.7	0.009
		R	0.34	0.31	0.22	13.05	0.009
	Middle temporal gyrus	L	0.32	0.28	0.23	11.97	0.001
		R	0.31	0.27	0.21	11.36	0.001
	Inferior temporal gyrus	L	0.33	0.30	0.20	11.83	<0.001
		R	0.32	0.28	0.19	11.94	<0.001
	Parahippocampal gyrus	L	0.45	0.43	0.19	NA	0.2
		R	0.44	0.43	0.18	NA	0.2
	Lingual gyrus	L	0.30	0.26	0.23	NA	0.5
		R	0.31	0.28	0.23	NA	0.6
	Fusiform gyrus	L	0.41	0.36	0.23	15.36	<0.001
		R	0.40	0.36	0.22	15.49	<0.001
Limbic lobe	Cingulate gyrus	L	0.37	0.34	0.24	12.42	0.02
		R	0.37	0.34	0.24	13.19	<0.001
	Hippocampus	L	0.34	0.30	0.23	NA	0.003
		R	0.35	0.32	0.24	NA	0.008
Others	Insular cortex	L	0.39	0.38	0.20	NA	0.05
		R	0.39	0.37	0.18	NA	0.3
	Caudate	L	0.41	0.42	0.28	NA	0.6
		R	0.43	0.44	0.29	NA	0.4
	Putamen	L	0.42	0.43	0.16	NA	0.05
		R	0.41	0.42	0.15	NA	0.04
	Cerebellum	NA	0.36	0.34	0.19	NA	0.2
	Brain stem	NA	0.44	0.45	0.15	NA	<0.001

[†]: r and ρ represent the Pearson and Spearman correlation coefficients, respectively. β_j represents the slope of the median absolute SUV for individual structure.